ChemComm

Intermediates and Mechanism in Iron-Catalyzed C-H Methylation with $AlMe_3$

Journal:	*ChemComm*
Manuscript ID	CC-COM-10-2021-005607.R1
Article Type:	Communication

COMMUNICATION

Received 00th January 20xx,
Accepted 00th January 20xx
DOI: 10.1039/x0xx00000x

Intermediates and Mechanism in Iron-Catalyzed C-H Methylation with Trimethylaluminum

Shilpa Bhatia, ‡ Joshua C. DeMuth, ‡ and Michael L. Neidig*

A mechanistic study is performed on the reaction method for iron-catalyzed C-H methylation with $AlMe_3$ reagent, previously proposed to involve cyclometalated iron(III) intermediates and an iron(III)/(I) reaction cycle. Detailed spectroscopic studies (^{57}Fe Mössbauer, EPR) during catalysis and in stoichiometric reactions identify iron(II) complexes, including cyclometalated iron(II) intermediates, as the major iron species formed in situ under catalytic reaction conditions. Reaction studies identify a cyclometalated iron(II)-methyl species as the key intermediate leading to C-H methylated product upon reaction with oxidant, consistent with a previously proposed iron(II)/iron(III)/iron(I) reaction manifold for C-H arylation.

While impressive advances in methods development in the field of iron-catalyzed C-H activation/functionalization have been achieved over the past two decades,[1-25] the underlying reaction mechanisms that enable effective catalysis in these systems remain poorly defined. Recently, a few noteworthy studies have started to address this challenge, providing key insight into the iron intermediates and reaction pathways involved in several of these methods.[26-28] In 2019, our group established the key on-cycle low-spin cyclometalated species in a triazole-assisted C-H arylation system, and determined that a low-spin iron-aryl species reacts with oxidant consistent with an iron(II)/iron(III)/iron(I) redox manifold.[26] In collaboration with Gutierrez and coworkers, these studies were later extended to an iron-catalyzed C-H allylation system, determining that the underlying reaction mechanism involves a low-spin, cyclometalated iron(II) intermediate that reacts with electrophile via an inner-sphere radical mechanism to form allylated product.[27] In addition, Ackermann and coworkers have also recently identified a key cyclometalated iron(II) hydride intermediate in iron-phosphine catalyzed C-H alkylation of arylphenones.[28]

While these recent mechanistic studies represent critical advances toward defining the key iron intermediates and reaction pathways involved in iron-catalyzed C-H activation/functionalization methods, all these reactions were found to involve cyclometalated iron(II) intermediates. However, alternative redox manifolds have been proposed in some iron-catalyzed C-H activation/functionalization reactions, including systems that may access low-valent iron catalysts or involve cyclometalated iron(III) intermediates.[13, 29-31] For the latter, Nakamura and coworkers have reported two C-H activation/functionalization methods that have been proposed to utilize cyclometalated iron(III) intermediates and follow an iron(III)/iron(I) cycle; quinoline-directed iron-catalyzed C-H alkylation and C-H arylation of benzamides with alkylaluminum nucleophiles and arylboronate reagents, respectively (Scheme 1).[29, 30] While the proposed iron(III) intermediates and iron(III)/(I) redox cycle in these systems would represent a unique reaction manifold compared to those currently defined, the proposals are based on sparse, preliminary experimental studies in which the key iron-intermediates and reactions pathways have not been directly evaluated.

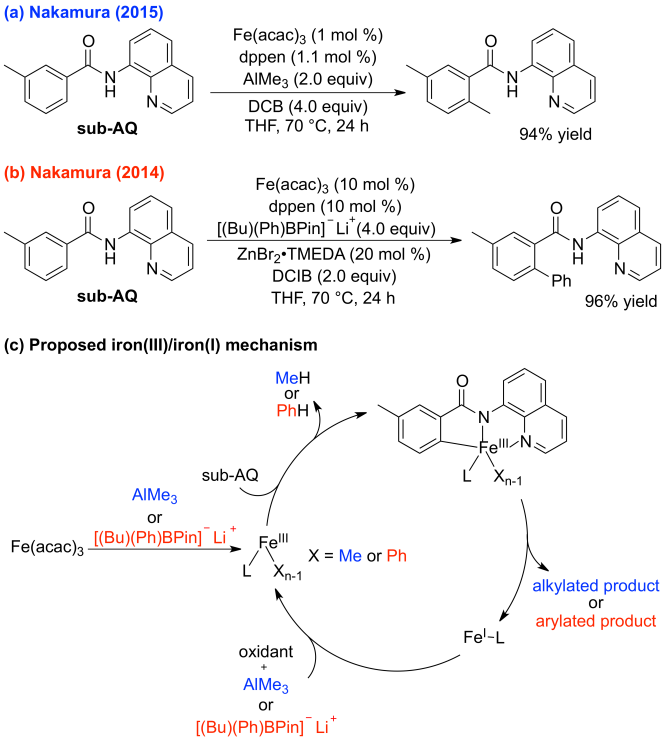

Scheme 1 Iron-catalyzed (a) C-H alkylation with organoaluminum reagents and (b) C-H arylation with organobornates. (c) The proposed iron(III)/iron(I) reaction mechanism utilizing cyclometalated iron(III) intermediates in these systems. (DCB = 2,3-dichlorobutane; DCIB = 1,2-dichloroisobutane)

Due to the importance of defining the breadth of catalytic manifolds that can be effective for iron-catalyzed C-H activation/functionalization methods, the current study utilizes detailed spectroscopic and reaction studies to interrogate the mechanism of iron-catalyzed C-H alkylation with organoaluminum reagents. These studies directly evaluate iron speciation and reaction pathways in these systems, including direct evaluation of the

Department of Chemistry, University of Rochester, Rochester, New York 14627, USA. E-mail: neidig@chem.rochester.edu
†Electronic Supplementary Information (ESI) available: [details of any supplementary information available should be included here]. See DOI: 10.1039/x0xx00000x
‡ These authors contributed equally.

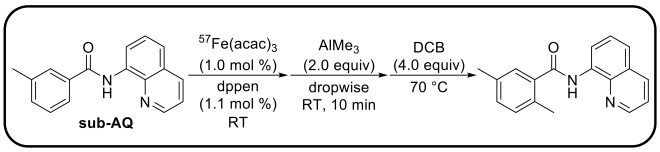

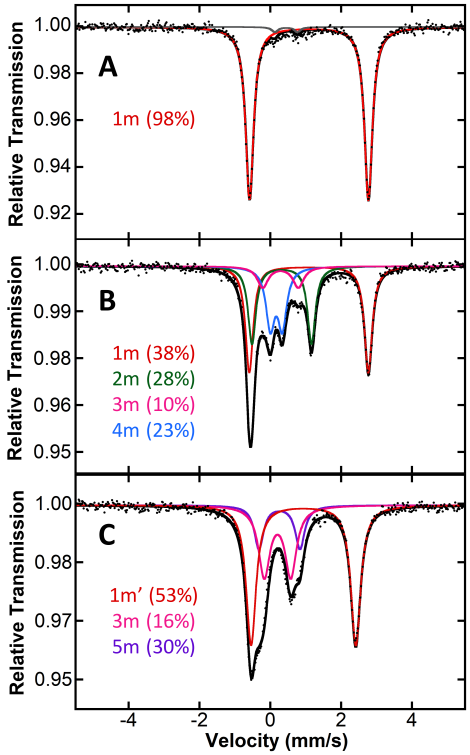

Fig. 1 Freeze-quenched 80 K ^{57}Fe Mossbauer spectra of the catalytic reaction (A) without oxidant at RT for 10 min (B) 5 min heating without oxidant and (C) 5 h heating with oxidant.

oxidation state of the cyclometalated iron intermediates (iron(III) as proposed or iron(II) as observed in other systems) central to effective catalysis in this system.

Our mechanistic investigations of C-H methylation of quinolinamides with $AlMe_3$ began with the assessment of the iron species formed in situ during catalysis. Following the published reaction protocol,[30] a solution of $Fe(acac)_3$ (iron(III) acetylacetonate) and dppen (1,2-bis(diphenylphosphino) ethylene) was added to a solution of aminoquinoline substrate (**sub-AQ**) in THF at room temperature (RT) with a subsequent addition of $AlMe_3$ at RT (Fig. 1, top). Freeze-quenched 80 K ^{57}Fe Mössbauer analysis revealed the formation of one major iron species **1m** with parameters δ = 1.09 mm/s and $|\Delta E_Q|$ = 3.35 mm/s (Figure 1A). These parameters are consistent with those of an analogous high-spin iron(II) amide-bound species **1a** previously observed in the triazole-assisted iron-catalyzed C-H arylation of benzamides (Table 1 and Scheme 2).[26] Thus, facile reduction to iron(II) has already occurred at this initial phase of the catalytic reaction protocol though no cyclometalated iron species have yet formed. However, subsequent heating of the solution to the catalytic reaction temperature (70 °C) for five minutes resulted in the partial consumption of **1m** and the presence of three new species **2m**, **3m**, and **4m** (Figure 1B). The Mössbauer parameters of **2m** and **3m** are consistent with previously observed cyclometalated low-spin iron(II) intermediates **2a** (contains THF adduct) and **3a** in the triazole-assisted C-H arylation system (Table 1).[26] The parameters of **4m** are similar to those of the aforementioned cyclometalated iron(II)-aryl

Table 1 80 K ^{57}Fe Mössbauer Parameters of Identified Iron Species

complex	sample	δ (mm/s)	$\|\Delta E_Q\|$ (mm/s)
Arylation System[a]			
1a	frozen soln	0.94	3.14
2a	frozen soln	0.30	1.92
	solid	0.30	1.90
3a	frozen soln	0.24	1.19
4a	frozen soln	0.15	0.54
This Work			
1m	frozen soln	1.09	3.35
2m	frozen soln	0.31	1.71
3m	frozen soln	0.29	0.99
4m	frozen soln	0.16	0.36

[a] *Values obtained from reference 26*

species **4a** (Table 1), consistent with its formation via transmetalation of **2m/3m** with $AlMe_3$.[26] These results suggest that heating promotes facile C-H activation and indicates that analogous cyclometalated iron(II) species to those observed in other iron-catalyzed C-H activation/functionalization systems can also be accessed in the current system. To define the iron species present during catalysis, the reaction was performed again with oxidant 2,3-dichlorobutane (DCB) at 70 °C. Freeze-trapped ^{57}Fe Mössbauer analysis after five hours of reaction revealed the formation of a high-spin iron(II) species **1m'** (δ = 0.95 mm/s and $|\Delta E_Q|$ = 2.96 mm/s), likely a product-bound analogue of **1m**, as well as a cyclometalated iron(II) complex **3m** and a new low-spin iron(II) species **5m** (δ = 0.21 mm/s and $|\Delta E_Q|$ = 0.74 mm/s) (Figure 1C). The new low-spin species **5m** could be identified by single-crystal X-ray diffraction, ^{1}H NMR, ^{31}P NMR, and ^{57}Fe Mössbauer analyses as $Fe(Me)_2(dppen)_2$ (ESI Figure S1-S3 and ESI Section 3). Lastly, corresponding 10 K EPR studies of all these reactions indicated less than 2 % EPR active species after 10 mins at RT and 5 mins at 70 °C and less than 0.1% EPR active species in the presence of oxidant, in the catalytic reaction at five hours, further consistent with the initial ferric iron being readily reduced and that the primary species present during catalysis are iron(II) complexes.

Having determined that predominantly iron(II) species were present during catalysis, additional stoichiometric reactions were performed to further investigate the formation of these complexes

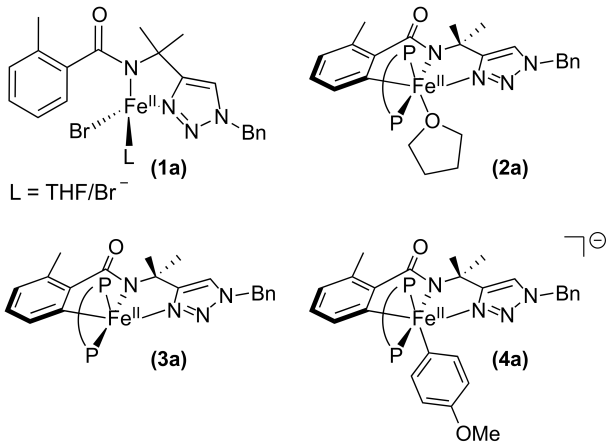

Scheme 2 Previously identified intermediates in triazole-assisted iron-catalyzed C-H arylation of benzamides.[26] (P-P = dppbz)

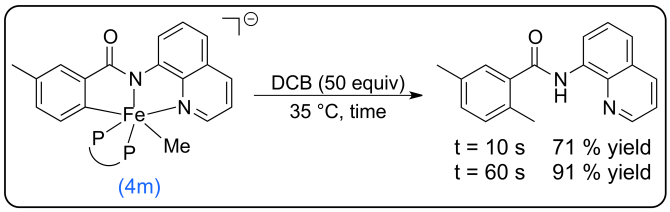

Scheme 3 Reaction of in situ generated **4m** with excess oxidant (DCB, 50 equiv) to generate ortho-C-H methylated product. Yield is with respect to the initial amount of **4m** and was quantified using ^{1}H NMR.

in situ. A stoichiometric reaction using Fe(acac)$_3$, 1 equiv of **sub-AQ**, 1.1 equiv of dppen and 1 equiv of AlMe$_3$ with initial reaction at RT followed by heating to 70 °C (i.e. the previously described catalytic protocol) was performed and subsequently freeze-trapped for Mössbauer analysis. However, instead of providing access to a single iron species, the resultant ^{57}Fe Mössbauer spectrum following five minutes of reaction revealed the formation of a complex mixture of iron(II) species including **2m**, **3m**, **4m**, and **5m** along with a high-spin iron(II) complex **6m** (see ESI Figure S5). Therfore, an additional stoichiometric reaction was performed at a reduced temperature to help facilitate the formation of a less complex mixture as well as avoid potential thermal decomposition pathways, as observed in our previous studies.[27] The reaction with one equivalent of AlMe$_3$ at 55 °C generated **1m** (4 % of total iron), **2m** (47 %), **3m** (30 %), and **6m** (18 %) (Figure S6). A corresponding ^{2}H NMR of this solution quenched in D$_2$O revealed aromatic deuterium incorporation consistent with the previous assignment of **2m** and **3m** as cyclometalated iron (II) species (Figure S7). Moreover, obtaining such iron distributions (including the formation of cyclometalated species whose formation requires multiple methyl equivalents) is indicative that all three methyl groups from AlMe$_3$ can be transferred in these reactions (see Figure S6 for additional substoichiometric reactions). These studies indicate that the first methyl group facilitates reduction of the ferric salt to a high-spin iron(II) complex, while subsequent methyl groups

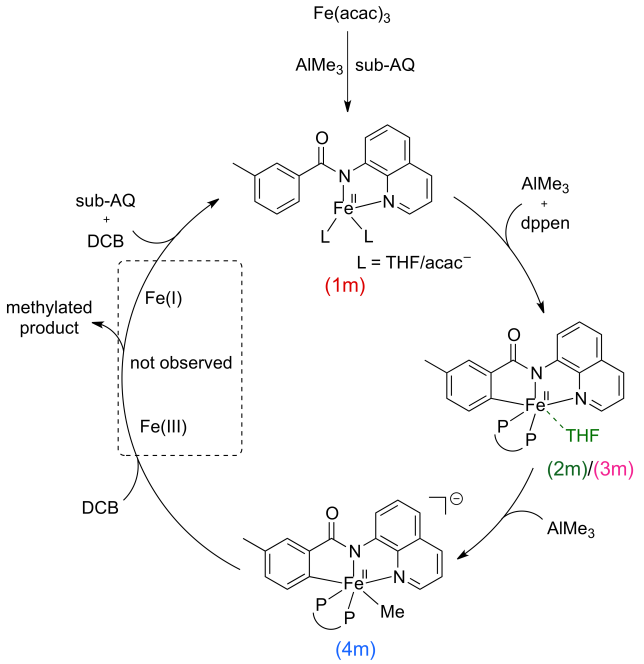

Scheme 4 Proposed mechanism for quinoline-directed iron-catalyzed C-H methylation of benzamides with trimethylaluminum based on spectroscopic and reactivity studies reported herein. (P-P = dppen)

promote amide deprotonation and C-H activation to generate cyclometalated species **2m** and **3m**. Intermediate **4m** (34 %) can be generated through the use of an additional third of an equivalent of AlMe$_3$ to enable further transmetalation of **2m/3m** to form an iron-methyl bond (Figure S6). Lastly, **4m** could alternatively be accessed in larger amounts (63 %) through the reaction of **sub-AQ**, Fe(acac)$_3$, and dppen, with four equivalents of MeMgBr (Figure S8).

Having established that the catalytic reaction generates iron(II) intermediates analogous to those of triazole-assisted C-H arylation, it was hypothesized that **4m** is potentially the key iron intermediate that reacts with oxidant to form methylated product, analogous to the role of **4a** inthe C-H arylation system.[26] To test this hypothesis, a reactivity study was performed by treating in situ generated **4m** (using MeMgBr as previously described) with excess oxidant (DCB, 50 equiv) at 35 °C (a temperature employed to minimize **4m** decomposition). The corresponding ^{57}Fe Mössbauer analysis revealed the consumption of **4m** upon addition of oxidant with a concomitant production of a high-spin iron(II) species (Figure S8), and a corresponding ^{1}H NMR analysis revealed that the *ortho*-C-H methylated product was formed in 91% yield with respect to the initial amount of **4m** (Scheme 3). Note, no additional product formation was observed beyond 60 seconds revealing that the reaction is completed by this time. These results indicate that **4m** promptly reacts (even at reduced temperatures) with oxidant to make the desired product, consistent with its assignment as the key cyclometalated iron-methyl intermediate likely following an iron(II)/iron(III)/iron(I) redox manifold as previously proposed in iron-catalyzed C-H arylation with triazole assistance (Scheme 4).

Lastly, while the current study indicates that iron-catalyzed C-H methylation with trimethylaluminum reagents also utilizes cyclometalated iron(II) intermediates to form methylated product in constrast to the previously proposed iron(III)/iron(I) mechanism, it was also interesting to consider if iron(II) is the dominate oxidation state for iron-catalyzed C-H arylation with arylboronate reagents (Scheme 1b) as this reaction was also proposed to utilize cyclometalated iron(III) intermediates. To evaluate this, freeze-trapped ^{57}Fe Mössbauer analysis was used to track the iron species present during catalysis at 70 °C of iron-catalyzed C-H arylation of **sub-AQ** with in situ generated phenylboronate reagent after one hour (Figure S9) and four hours (Figure 2) of reaction. These studies revealed the in situ formation of high-spin iron(II) species as well as additional iron compounds with parameters suggestive of low-spin cyclometalated iron(II) complexes (Note that the blue component is

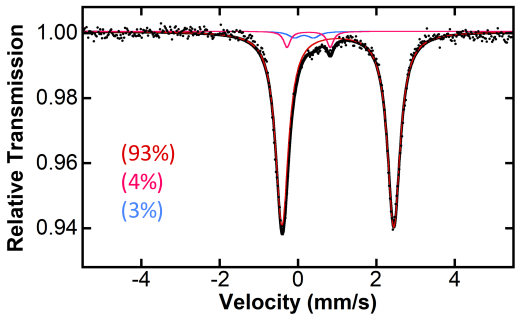

Fig. 2 80 K ^{57}Fe Mössbauer analysis of iron-catalyzed C-H arylation of **sub-AQ** with a phenylboronate reagent after four hours of reaction. The corresponding 5 K EPR analysis revealed the major iron species is EPR silent. The individual component parameters are the following: (a) red component, δ = 1.02 mm/s and $|\Delta E_Q|$ = 2.80 mm/s, (b) pink component, δ = 0.27 mm/s and $|\Delta E_Q|$ = 1.10 mm/s and (c) blue component, 0.16 mm/s and $|\Delta E_Q|$ = 0.47 mm/s.

the major iron species at one hour, see Figure S9). Thus, these preliminary studies suggest that dominance of iron(II) species during catalysis, indicating that cyclometalated iron(II) intermediates are likely also operative for C-H arylation with arylboronate reagents.

In conclusion, iron-catalyzed C-H methylation with trimethylaluminum was found to predominantly access iron(II) species during catalysis that are analogous to those previously identified in triazole-assisted C-H arylation. Critically, a low-spin cyclometalated iron(II) intermediate was identified that reacts with oxidant to generate C-H methylated product consistent with an iron(II)/iron(III)/iron(I) reaction manifold. In addition, iron-catalyzed C-H arylation with arylboronate reagents accesses iron(II) species during catalysis implicating that a reaction manifold involving iron(II) intermediates may be operative as well. These results contrast previous proposals for cyclometalated iron(III) intermediates and an iron(III)/iron(I) manifold for these reactions, further defining the central role of cyclometalated iron(II) intermediates across a wide range of C-H activation/functionalization systems. Overall, these studies continue to expand and develop a mechanistic foundation for this important class of reactions in order to enable the rational design of the next generation of iron-catalysts for C-H activation/functionalization.

Conflicts of interest

The authors declare no conflicts of interest.

Acknowledgements

This work was supported by a grant from the National Science Foundation (CHE-1954480 to M.L.N.). We thank William. W. Brennessel for assistance with X-ray crystallography.

Notes and references

1. S. Asako, L. Ilies and E. Nakamura, *J. Am. Chem. Soc.*, 2013, **135**, 17755-17757.
2. S. Asako, J. Norinder, L. Ilies, N. Yoshikai and E. Nakamura, *Adv. Synth. Catal.*, 2014, **356**, 1481-1485.
3. G. Cera, T. Haven and L. Ackermann, *Angew. Chem. Int. Ed.*, 2016, **55**, 1484-1488.
4. G. Cera, T. Haven and L. Ackermann, *Chem. Eur. J.*, 2017, **23**, 3577-3582.
5. E. R. Fruchey, B. M. Monks and S. P. Cook, *J. Am. Chem. Soc.*, 2014, **136**, 13130-13133.
6. K. Graczyk, T. Haven and L. Ackermann, *Chem. Eur. J.*, 2015, **21**, 8812-8815.
7. N. Kimura, S. Katta, Y. Kitazawa, T. Kochi and F. Kakiuchi, *J. Am. Chem. Soc.*, 2021, **143**, 4543-4549.
8. N. Kimura, T. Kochi and F. Kakiuchi, *Asian J. Org. Chem.*, 2019, **8**, 1115-1117.
9. J. Loup, D. Zell, J. C. A. Oliveira, H. Keil, D. Stalke and L. Ackermann, *Angew. Chem. Int. Ed.*, 2017, **56**, 14197-14201.
10. B. M. Monks, E. R. Fruchey and S. P. Cook, *Angew. Chem. Int. Ed.*, 2014, **53**, 11065-11069.
11. R. Shang, L. Ilies and E. Nakamura, *J. Am. Chem. Soc.*, 2016, **138**, 10132-10135.
12. Z. Shen, G. Cera, T. Haven and L. Ackermann, *Org. Lett.*, 2017, **19**, 3795-3798.
13. M. Y. Wong, T. Yamakawa and N. Yoshikai, *Org. Lett.*, 2015, **17**, 442-445.
14. Q. Gu, H. H. Al Mamari, K. Graczyk, E. Diers and L. Ackermann, *Angew. Chem. Int. Ed.*, 2014, **53**, 3868-3871.
15. L. Ilies, S. Asako and E. Nakamura, *J. Am. Chem. Soc.*, 2011, **133**, 7672-7675.
16. L. Ilies, Y. Itabashi, R. Shang and E. Nakamura, *ACS Catal.*, 2017, **7**, 89-92.
17. L. Ilies, E. Konno, Q. Chen and E. Nakamura, *Asian J. Org. Chem.*, 2012, **1**, 142-145.
18. J. Norinder, A. Matsumoto, N. Yoshikai and E. Nakamura, *J. Am. Chem. Soc.*, 2008, **130**, 5858-5859.
19. R. Shang, L. Ilies, A. Matsumoto and E. Nakamura, *J. Am. Chem. Soc.*, 2013, **135**, 6030-6032.
20. J. J. Sirois, R. Davis and B. DeBoef, *Org. Lett.*, 2014, **16**, 868-871.
21. N. Yoshikai, A. Matsumoto, J. Norinder and E. Nakamura, *Angew. Chem. Int. Ed.*, 2009, **48**, 2925-2928.
22. G. Cera, T. Haven and L. Ackermann, *Chem. Commun.*, 2017, **53**, 6460-6463.
23. L. Ilies, Y. Arslanoglu, T. Matsubara and E. Nakamura, *Asian J. Org. Chem.*, 2018, **7**, 1327-1329.
24. L. Ilies, A. Matsumoto, M. Kobayashi, N. Yoshikai and E. Nakamura, *Synlett*, 2012, **23**, 2381-2384.
25. T. Jia, C. Zhao, R. He, H. Chen and C. Wang, *Angew. Chem. Int. Ed.*, 2016, **55**, 5268-5271.
26. T. E. Boddie, S. H. Carpenter, T. M. Baker, J. C. DeMuth, G. Cera, W. W. Brennessel, L. Ackermann and M. L. Neidig, *J. Am. Chem. Soc.*, 2019, **141**, 12338-12345.
27. J. C. DeMuth, Z. Song, S. H. Carpenter, T. E. Boddie, A. Radović, T. M. Baker, O. Gutierrez and M. L. Neidig, *Chem. Sci.*, 2021, **12**, 9398-9407.
28. A. M. Messinis, L. H. Finger, L. Hu and L. Ackermann, *J. Am. Chem. Soc.*, 2020, **142**, 13102-13111.
29. R. Shang, L. Ilies, S. Asako and E. Nakamura, *J. Am. Chem. Soc.*, 2014, **136**, 14349-14352.
30. R. Shang, L. Ilies and E. Nakamura, *J. Am. Chem. Soc.*, 2015, **137**, 7660-7663.
31. N. Kimura, T. Kochi and F. Kakiuchi, *J. Am. Chem. Soc.*, 2017, **139**, 14849-14852.